CHINESE OPTICS LETTERS

Vol. 20, No. 10 | October 2022

Layer-dependent photoexcited carrier dynamics of WS_2 observed using single pulse pump probe method

Lin Zhang (张 林)[1], Jiamin Liu (刘佳敏)[1], Hao Jiang (江 浩)[1*], Honggang Gu (谷洪刚)[1], and Shiyuan Liu (刘世元)[1,2**]

[1] State Key Laboratory of Digital Manufacturing Equipment and Technology, Huazhong University of Science and Technology, Wuhan 430074, China

[2] Optics Valley Laboratory, Wuhan 430074, China

*Corresponding author: hjiang@hust.edu.cn

**Corresponding author: shyliu@hust.edu.cn

Received April 11, 2022 | Accepted June 16, 2022 | Posted Online August 3, 2022

Understanding the ultrafast carrier dynamics and the mechanism of two-dimensional (2D) transition metal dichalcogenides (TMDs) is key to their applications in the field of optoelectronic devices. In this work, a single pulse pump probe method is introduced to detect the layer-dependent ultrafast carrier dynamics of monolayer and few-layer WS_2 excited by a femtosecond pulse. Results show that the ultrafast carrier dynamics of the layered WS_2 films can be divided into three stages: the fast photoexcitation phase with the characteristic time of 2–4 ps, the fast decay phase with the characteristic time of 4–20 ps, and the slow decay phase lasting several hundred picoseconds. Moreover, the layer dependency of the characteristic time of each stage has been observed, and the corresponding mechanism of free carrier dynamics has been discussed. It has been observed as well that the monolayer WS_2 exhibits a unique rising time of carriers after photoexcitation. The proposed method can be expected to be an effective approach for studying the dynamics of the photoexcited carriers in 2D TMDs. Our results provide a comprehensive understanding of the photoexcited carrier dynamics of layered WS_2, which is essential for its application in optoelectronics and photovoltaic devices.

Keywords: photoexcited carrier; pump probe; 2D material; single pulse measurement.

DOI: 10.3788/COL202220.100002

1. Introduction

Transition metal dichalcogenides (TMDs) have attracted tremendous attention and played an important role in the development of two-dimensional (2D) semiconductor materials in the past decade due to their unique physical properties and outstanding photoelectric performance[1–3]. The extraordinary physical properties of the TMDs can be attributed to their unique physical structure. TMDs are layered structures, in which monolayer materials are stacked together through weak van der Waals forces between layers[4]. As a result, the optical and physical properties of TMDs will always exhibit striking layer-dependent evolutions[5,6]. Peculiarly, when the material is thinned from multiple layers to an atomically thin monolayer, the indirect band gap semiconductor will be transformed into a direct band gap semiconductor[7]. Due to its fascinating and layer-dependent photoelectronic and mechanical properties, 2D TMDs have promising potential applications in the field of optoelectronics, electronics, and flexible devices[8–11].

As one of the most studied materials in the family of TMDs, tungsten disulphide (WS_2) has been widely used in the field of highly responsive photosensors and electrics devices. A deep understanding of the ultrafast carrier dynamics of WS_2 and the corresponding mechanisms upon photoexcitation is the prerequisites for its applications. Therefore, many time-domain studies have been carried out on the photoexcited carrier dynamics of WS_2 and MoS_2 utilizing transient absorption spectroscopy[2,12,13], photoemission electron microscopy[12,14–16], time-resolved photoluminescence[17], and time-resolved terahertz (THz) spectroscopy[18,19], and so on. As a result, the transient excitation process of the carriers with the time scale from several hundred femtoseconds (fs) to picoseconds, and the subsequent carrier decay process with the time scale from tens of picoseconds to nanoseconds, were studied. The decay process of the photoexcited carriers, which occupies most of the time of the carrier responses, has been divided into two[18,20,21] or three[2,12,22] stages for mechanism explanation in different works. Correspondingly, different explanations for the carrier decay process have been reported such as carrier thermalization and cooling[23], exciton formation, dissociations and annihilations[17,24,25], defect-assisted electron hole recombination[20], Auger scattering[12], and electron–phonon interaction[26]. These differences may be due to the various detection devices or the different sample preparation methods[14,27]. Therefore,

more efforts are still needed to bring us more information, which is critical to building a comprehensive understanding of the photoexcited carrier dynamics and the corresponding mechanisms in layered WS_2.

It is well known that, in the measurement of dynamic processes on ultrafast time scales, the reported methods include multi-shot methods[11,13,17,28] and single-shot methods[29–31]. In the measurements of photoexcited carrier dynamics, due to the instability of the output pulse and the inhomogeneity of the sample, non-negligible uncertainties and systematic errors to the results will be inevitably introduced from the data collected in different shots. Therefore, the single-shot method can provide more reliable results compared with the multi-shot method. Besides, most of the existing studies focus on various optoelectronic properties of monolayer materials. While understanding the layer-dependent photoexcited carrier dynamics of layered WS_2 is a crucial step for expanding its applications, in this paper, a single pulse method based on the pump probe technique is proposed to detect the ultrafast carrier dynamics of layered WS_2 from 1 to 5 layers excited by a fs pulse with pump fluence of 1 mJ/cm^2. The spatiotemporal spectrum of the photoexcited carrier dynamics can be obtained in a single measurement by employing the linear chirped pulse as the probe light. From the spectrum, the ultrafast carrier dynamics can be obtained, including the fast photoexcitation phase with characteristic time of 2–4 ps, the fast decay phase with characteristic time of 4–20 ps, and the slow decay phase lasting several hundred picoseconds. Further, the layer dependency of the characteristic time of each stage has been demonstrated, and the corresponding mechanism of free carrier dynamics has been discussed.

2. Experiments

The WS_2 samples were obtained through commercial purchase (6Carbon Technology), prepared using the chemical vapor deposition (CVD) method. The substrate is sapphire with a thickness of 0.3 mm. Figure 1(a) shows the optical image of the three-layer WS_2 with size of 10 mm × 10 mm. A Raman spectrometer (inVia Reflex) is used to analyze the Raman spectra, and the excitation wavelength is set as 532 nm. Figure 1(b) shows the Raman spectra at different marked positions, shown as Fig. 1(a). Two characteristic peaks (E^1_{2g} and A_{1g}) in the spectrum are observed, which represent two kinds of phonon vibration modes (in-plane and out-of-plane, respectively). The position differences between the two peaks maintain 61.5 cm^{-1} in five measurements, which means that the thickness uniformity of the sample is good. The Raman spectra of the WS_2 from monolayer to five layers are shown in Figs. 1(c)–1(e), respectively. The position difference between peak E^1_{2g} and peak A_{1g} shows a dependence on the number of layers, which is consistent with previous reports[17,32]. In addition, extremely small surface roughness indicates excellent surface quality of the samples, shown in the atomic force microscopy (AFM, SPM9700, Shimadzu) results, as shown in Figs. 1(f)–1(h).

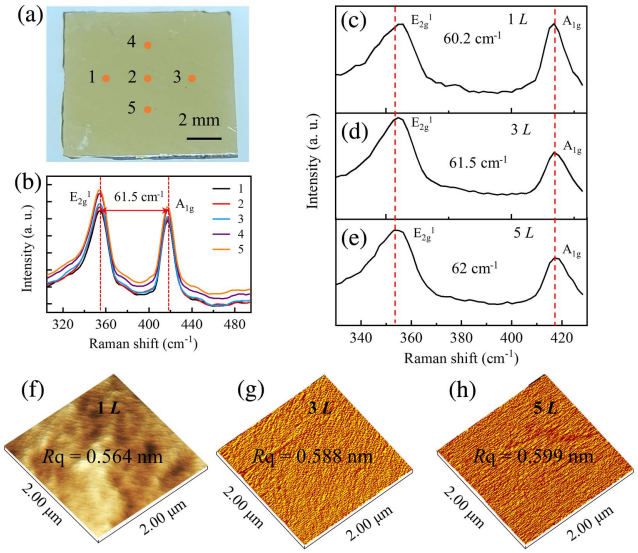

Fig. 1. Characterization of the WS_2 films with different layers used in this study. (a) Optical image of sample with size of 10 mm × 10 mm. The WS_2 film was plated on a 0.3 mm sapphire substrate by the CVD method. (b) Raman spectra of the three-layer WS_2 at different points. (c)–(e) Raman spectra of WS_2 films with 1–5 layers. (f)–(h) The surface roughness of the 1L, 3L, and 5L samples characterized by AFM.

The schematic diagram of the proposed single pulse pump probe method is shown in Fig. 2(a), which is similar to the configuration in our previous work[29]. A Ti:sapphire laser (Newport Corporation, SOL-ACE35F1K-HP) is employed to deliver 35 fs Gaussian limit pulses with central wavelength of 800 nm and maximum single pulse energy of ~7 mJ. The repetition rates of the output pulse of the system are set as

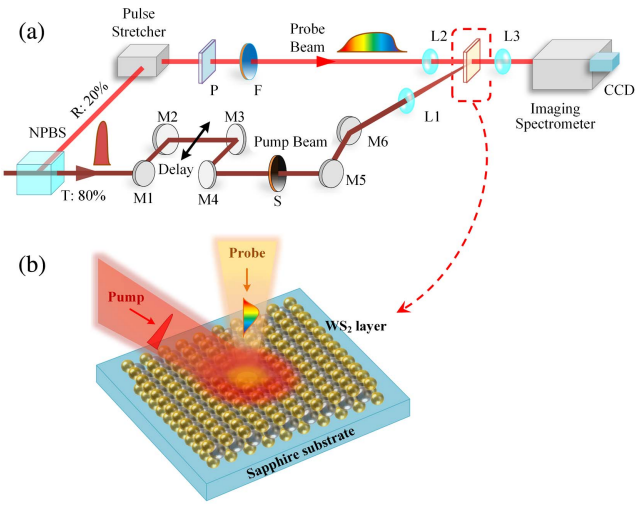

Fig. 2. (a) Schematic diagram of the pump-probe-based optical configuration. (b) Schematic diagram of the marked area in (a). The probe light spot size is smaller than the pump light spot and falls in the center of the pump light spot on the sample. NPBS, non-polarized beam splitter; P, polarizer; F, neutral filter wheel; M, mirror; S, mechanical shutter; L, lens.

10 Hz. The output fs pulse is divided into two beams by a non-polarized beam splitter (NPBS). The beam with 80% pulse energy is used as the pump beam to excite the sample at an incident of 45° through a focusing lens (ACA254-150-B, Thorlabs) with a focal length of 150 mm. The pump fluence of the single pulse can reach ~1 mJ/cm^2 on the sample. A mechanical shutter (SH1/M, Thorlabs) with open time of 0.1 s is used to ensure that only one pulse is used in a single measurement. Meanwhile, the beam with 20% pulse energy enters a home-made grating-based pulse stretcher, which converts the fs pulse into a linearly chirped pulse. The linear relationship between the wavelength and time of the stretched pulse can be expressed as $\lambda = 0.1124t + 786.2$, where 0.1124 is the linear coefficient with unit of nm/ps. The details of the pulse stretcher and the chirp parameters measurement can be found in Ref. [33]. The chirped pulse transits a polarizer to generate a p-polarized light. A neutral filter wheel with a variable filter ratio is used in the probe path to protect the detector. A delay line is used to ensure the synchronism between the probe light and the pump light. An achromatic lens (ACA254-075-B, Thorlabs) with focal length of 75 mm is employed to focus the probe beam, resulting in a spot size of about 1 mm at the detection point, which is smaller than the spot diameter of the focused pump beam (2 mm). The details at the detection point are shown in Fig. 2(b). The pump light intensity on the irradiating area of the probe light presents a Gaussian distribution under the precondition that the probe spot is located at the center of the pump area. Through another achromatic lens (ACA254-050-B, Thorlabs) with focal length of 50 mm, the excited area of the sample is imaged onto the slit of an imaging spectrometer (Horiba, iHR550). The width of the entrance slit of the imaging spectrometer is set as 0.016 mm. As a result, a spectrum containing the dynamic responses of the sample after excitation will be recorded on the CCD detector (Horiba, Syncer-1024 × 256). A process duration of 282 ps can be recorded through one measurement, which is calculated from the chirped coefficient and the CCD spectral range (~31.7 nm), and the corresponding time resolution of the pump probe system is ~0.28 ps.

3. Results and Discussion

The experiment of the photoexcited free carrier dynamics of WS_2 is performed at room temperature. It is worth noting that the pulse energy fluctuation will introduce non-negligible measurement errors and even affect the observation of dynamic signals. However, such effects could be minimized by the single-shot strategy because all the data are collected in one test. Based on the above experimental conditions, Fig. 3(a) shows the measured static spectrum I_0 (without pump) and dynamic spectrum I_1 (with pump), where the wavelength dimension has been mapped into the time domain. It should be noted that the spectra shown in Fig. 3 are the results of the three-layer WS_2 sample. Obviously, it can be seen that the transmitted light intensity of the probe beam drops rapidly at the moment of pump excitation, as marked in Fig. 3(a). The decrease in transmitted intensity may be due to the enhanced absorption of the probe light by the sample. Through differential processing, a spectrum containing the dynamic evolution information at the detecting area can be obtained as Fig. 3(b). The horizontal black dashed line represents $\Delta I/I_0 = 0$, where $\Delta I = I_0 - I_1$. The open circles are the measured data, and the solid line represents the corresponding fitting result using a biexponential function, which can be described as

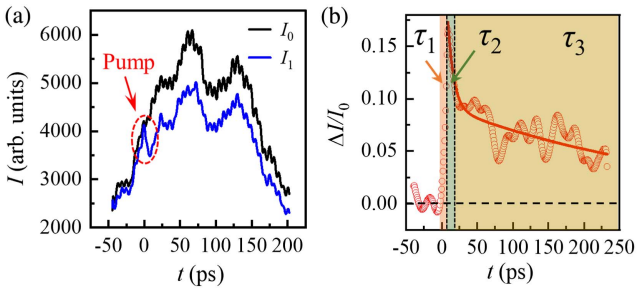

Fig. 3. (a) Static spectrum I_0 (black line) and dynamic spectrum I_1 (blue line). The time of pump excitation is marked. (b) Spectrum after differential processing. The open circles are the measured data, and the solid line represents the corresponding fitting result using a biexponential function. The spectra shown in this figure are the results of the three-layer WS_2 sample.

$$y = A_1 \exp(-t/\tau_2) + A_2 \exp(-t/\tau_3) + y_0, \tag{1}$$

where t is the time variable; τ_2 and τ_3 represent the carrier decay characteristic times, respectively. Equation (1) describes how the value $\Delta I/I_0$ decays from the peak to zero. Three distinct phases can be observed from the differential spectrum with characteristic times of τ_1, τ_2, and τ_3. Here, we name them as the fast photoexcitation phase, the fast decay phase, and the slow decay phase, respectively. First of all, the value of $\Delta I/I_0$ rises from zero to the maximum within ~4 ps after the pump induced photoexcitation. Then, a fast decay process of $\Delta I/I_0$ occurs within $\tau_2 = 8.4$ ps. Finally, a slow decay process of $\Delta I/I_0$ lasts for $\tau_3 = 338.1$ ps. It is worth mentioning that due to the limitation of the time range of the measured spectrum, the characteristic times of τ_2 and τ_3 were obtained by fitting Eq. (1) with the measured data.

In order to further reveal the layer dependency of the dynamic response of WS_2 being excited, the fs pump probe experiments were performed on WS_2 samples with different numbers of layers. Figure 4 shows the temporal evolution of the transmitted light intensity extracted from the measured spectrum, where the WS_2 layers are 1L, 3L, and 5L. Since the change of the probe light intensity is proportional to the carrier population changes[3], the evolution of the signal $\Delta I/I_0$ reflects the dynamics of the photoexcited carriers. In Fig. 4, the open circles are the measured data, and the solid lines represent the corresponding fitting results using the biexponential function. Obviously, the temporal evolution of the probe light intensity heavily depends on the number of layers. As the WS_2 layer number increases from 1L to 5L, the value of $\Delta I/I_0$ gradually increases, which indicates the increase of the number of photoexcited carriers, as well.

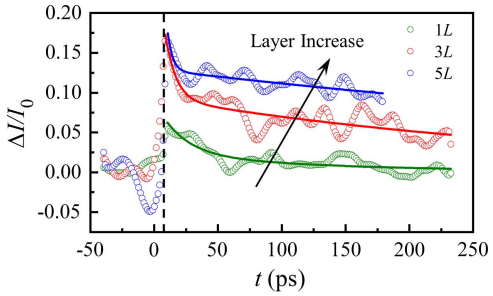

Fig. 4. Temporal evolution of the transmitted probe light intensity $\Delta I/I_0$ of the WS_2 films with different layers (1L, 3L, and 5L). The open circles are extracted from the measured spectrum, and the solid lines are the results of fitting using a biexponential function.

Then, the layer dependency of the characteristic time for the three phases in the dynamic response of the carriers is discussed. First, the relationship between the fast carrier excitation time τ_1 and the layers is shown in Fig. 5(a). It can be found that the carrier excitation time of monolayer WS_2 ($\tau_1 = 2.9$ ps) is significantly shorter than that of multilayer films (~4.1 ps), and no obvious trend can be concluded. The characteristic times for decay processes (τ_2 and τ_3) of WS_2 with different layers that are extracted from the biexponential function fitting process are shown in Table 1. Correspondingly, Figs. 5(b) and 5(c) show the layer dependence of τ_2 and τ_3. It can be observed that the fast decay phase is on the time scale from several picoseconds to tens of picoseconds, while the slow decay phase is in the scale of hundreds of picoseconds. The solid lines are the fitting results using

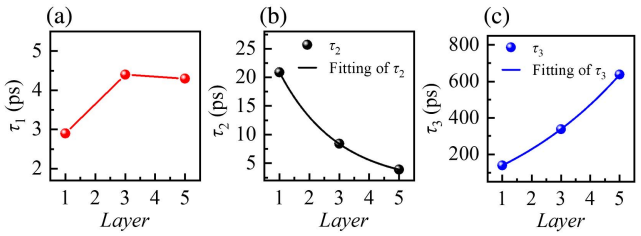

Fig. 5. (a) Characteristic time of the carrier excitation process as a function of the material layers. (b) The layer dependence of the carrier fast decay characteristic time and (c) the slow decay characteristic time in the process of carrier decay. The corresponding solid lines in (b) and (c) are the fitting results using an exponential function.

Table 1. The Characteristic Times τ_2 and τ_3 of Different Layers.

	Layers		
Parameters	**1L**	**3L**	**5L**
τ_2/ps	20.9	8.4	3.9
τ_3/ps	139.2	338.1	673.4

an exponential function. Obviously, the characteristic time τ_2 of the fast decay phase has an exponential decay trend with the layers. In contrast, the characteristic time τ_3 of the slow decay phase increases exponentially as the number of layers increases.

It is worth noting that the characteristic time of the carrier dynamic response (the rise and decay) obtained in our experiment is longer than the results reported in Refs. [18,21], which may be attributed to the relatively high pump pulse fluence used in our work[20].

We now discuss the mechanism that contributes to the observed phenomenon. First, we can start with the fast photoexcitation phase with characteristic time $\tau_1 = 2$–4 ps. The WS_2 films absorb the photon energy, and the electrons transition from the valence band to the conduction band once the pump pulse irradiates on the sample surface. During this process, the carrier generation rate is much faster than the carrier recombination rate, and a large number of electrons and holes accumulate at the bottom of the conduction band and on the top of the valence band, respectively. The existence of these hot carriers inevitably makes the system partly in a non-equilibrium state. Therefore, these unstable electrons and holes need to release their own energy to balance the system. Next, we consider the mechanism of the fast decay phase of the hot carrier with characteristic time $\tau_2 = 4$–20 ps. Theoretical predictions of the radiative recombination time are on the nanosecond scale[34,35], which is much longer than our results. The radiative recombination of the thermalized electrons and holes then can be excluded. Therefore, the non-radiative recombination is considered to be the dominant way[20,21]. To be more specific, the aforementioned fast decay phase within 20 ps can be attributed to the fast Auger recombination. During this process, the photoexcited carriers transfer energy to the phonon system through Auger recombination, which results in an increase of local lattice temperature. Finally, we come to the slow decay phase of the photoexcited carriers, whose characteristic time is on the scale of hundreds of picoseconds. The carrier population decreases rapidly due to the fast recombination of electron–hole pairs in the previous process, leading to a gradual decrease in the recombination rate of carriers. In addition, accompanying this recombination process is lattice cooling, the energy of which is dissipated in the form of thermal diffusion.

Further, we may try to explain the mechanism of the layer dependency of the characteristic time for the decay processes. It can be observed from Figs. 5(b) and 5(c) that the characteristic time of the fast decay phase τ_2 decreases exponentially with the increase of the layer number. In other words, the carrier recombination rate increases as the number of layers increases. Conversely, the characteristic time τ_3 of the slow recombination phase increases exponentially with the increase of the layer number. Such phenomena may be explained from the perspective of the photoexcited carrier numbers. As the number of layers increases, more carriers will be excited by the radiated pump pulse, which induce the increase of the carrier recombination rate. By the same token, the increase in the carrier number will take longer to pair the electron–hole and finally reach an equilibrium state.

4. Conclusion

In summary, a pump probe method has been proposed to study the ultrafast carrier dynamics of monolayer and few-layer WS_2 excited by a fs pump pulse with fluence of ~1 mJ/cm^2. It has been demonstrated that with the configuration proposed in our work, the dynamics of the photoexcited carriers within 282 ps can be obtained. Moreover, the layer dependency of the characteristic time of WS_2 carrier dynamics has been studied. Results show that the monolayer WS_2 exhibits a unique photoexcitation time, while the layer dependency of the photoexcitation time for the multilayer material is not observed. The carrier recombination stage shows a strong layer dependency. In addition, Auger recombination is considered to be the main mechanism of carrier recombination. The proposed method in this work is expected to be an effective approach to explore the ultrafast dynamics of photoexcited carriers in 2D semiconductor materials. This work also provides a further understanding of the mechanism of the photoexcited carrier dynamics of layered WS_2, which is the prerequisite for applying TMDs in the field of photoelectronic and photovoltaic devices.

Acknowledgement

This work was supported by the National Natural Science Foundation of China (Nos. 51975232 and 51727809). The authors thank the Experiment Center for Advanced Manufacturing and Technology in the School of Mechanical Science & Engineering of HUST for the technical support.

References

1. C. Cong, J. Shang, Y. Wang, and T. Yu, "Optical properties of 2D semiconductor WS_2," Adv. Opt. Mater. **6**, 1700767 (2018).
2. R. K. Chowdhury, S. Nandy, S. Bhattacharya, M. Karmakar, S. N. B. Bhaktha, P. K. Datta, A. Taraphder, and S. K. Ray, "Ultrafast time-resolved investigations of excitons and biexcitons at room temperature in layered WS_2," 2D Mater. **6**, 015011 (2018).
3. T. Zhu, J. M. Snaider, L. Yuan, and L. Huang, "Ultrafast dynamic microscopy of carrier and exciton transport," Annu. Rev. Phys. Chem. **70**, 219 (2019).
4. K. S. Novoselov, D. Jiang, F. Schedin, T. J. Booth, V. V. Khotkevich, S. V. Morozov, and A. K. Geim, "Two-dimensional atomic crystals," Proc. Natl. Acad. Sci. USA **102**, 10451 (2005).
5. H. Gu, B. Song, M. Fang, Y. Hong, X. Chen, H. Jiang, W. Ren, and S. Liu, "Layer-dependent dielectric and optical properties of centimeter-scale 2D WSe_2: evolution from a single layer to few layers," Nanoscale **11**, 22762 (2019).
6. B. Song, H. Gu, M. Fang, Y.-T. Ho, X. Chen, H. Jiang, and S. Liu, "Complex optical conductivity of 2D MoS_2: a striking layer-dependency," J. Phys. Chem. Lett. **10**, 6246 (2019).
7. K. F. Mak, C. Lee, J. Hone, J. Shan, and T. F. Heinz, "Atomically thin MoS_2: a new direct-gap semiconductor," Phys. Rev. Lett. **105**, 136805 (2010).
8. L. Gao, "Flexible device applications of 2D semiconductors," Small **13**, 1603994 (2017).
9. D. Jariwala, V. K. Sangwa, L. J. Lauhon, T. J. Marks, and M. C. Hersam, "Emerging device applications for semiconducting two-dimensional transition metal dichalcogenides," ACS Nano **8**, 1102 (2014).
10. B. W. Baugher, H. O. Churchill, Y. Yang, and P. Jarillo-Herrero, "Optoelectronic devices based on electrically tunable p-n diodes in a monolayer dichalcogenide," Nat. Nanotechnol. **9**, 262 (2014).
11. T. Yang, H. Lin, and B. Jia, "Ultrafast direct laser writing of 2D materials for multifunctional photonics devices [Invited]," Chin. Opt. Lett. **18**, 023601 (2020).
12. T. Jiang, R. Chen, X. Zheng, Z. Xu, and Y. Tang, "Photo-induced excitonic structure renormalization and broadband absorption in monolayer tungsten disulphide," Opt. Express **26**, 859 (2018).
13. P. Schiettecatte, P. Geiregat, and Z. Hens, "Ultrafast carrier dynamics in few-layer colloidal molybdenum disulfide probed by broadband transient absorption spectroscopy," J. Phys. Chem. C **123**, 10571 (2019).
14. Y. Li, W. Liu, Y. Wang, Z. Xue, Y. C. Leng, A. Hu, H. Yang, P. H. Tan, Y. Liu, H. Misawa, Q. Sun, Y. Gao, X. Hu, and Q. Gong, "Ultrafast electron cooling and decay in monolayer WS_2 revealed by time- and energy-resolved photoemission electron microscopy," Nano Lett. **20**, 3747 (2020).
15. A. Hu, W. Liu, X. Li, S. Xu, Y. Li, Z. Xue, J. Tang, L. Ye, H. Yang, M. Li, Y. Ye, Q. Sun, Q. Gong, and G. Lu, "Spectromicroscopy and imaging of photoexcited electron dynamics at in-plane silicon pn junctions," Nanoscale **13**, 2626 (2021).
16. W. Zheng, P. Jiang, L. Zhang, Y. Wang, Q. Sun, Y. Liu, Q. Gong, and C. Wu, "Ultrafast extreme ultraviolet photoemission electron microscope," Rev. Sci. Instrum. **92**, 043709 (2021).
17. L. Yuan and L. Huang, "Exciton dynamics and annihilation in WS_2 2D semiconductors," Nanoscale **7**, 7402 (2015).
18. X. Xing, L. Zhao, Z. Zhang, X. Liu, K. Zhang, Y. Yu, X. Lin, H. Y. Chen, J. Q. Chen, Z. Jin, J. Xu, and G.-h. Ma, "Role of photoinduced exciton in the transient terahertz conductivity of few-layer WS_2 laminate," J. Phys. Chem. C **121**, 20451 (2017).
19. J. K. Gustafson, P. D. Cunningham, K. M. McCreary, B. T. Jonker, and L. M. Hayden, "Ultrafast carrier dynamics of monolayer WS_2 via broadband time-resolved terahertz spectroscopy," J. Phys. Chem. C **123**, 30676 (2019).
20. H. Wang, C. Zhang, and F. Rana, "Ultrafast dynamics of defect-assisted electron-hole recombination in monolayer MoS_2," Nano Lett. **15**, 339 (2015).
21. C. Ruppert, A. Chernikov, H. M. Hill, A. F. Rigosi, and T. F. Heinz, "The role of electronic and phononic excitation in the optical response of monolayer WS_2 after ultrafast excitation," Nano Lett. **17**, 644 (2017).
22. Z. Chi, H. Chen, Q. Zhao, and Y. X. Weng, "Observation of the hot-phonon effect in monolayer MoS_2," Nanotechnology **31**, 235712 (2020).
23. Z. Nie, R. Long, L. Sun, C. C. Huang, J. Zhang, Q. Xiong, D. W. Hewak, Z. Shen, O. V. Prezhdo, and Z. H. Loh, "Ultrafast carrier thermalization and cooling dynamics in few-layer MoS_2," ACS Nano **8**, 10931 (2014).
24. V. Vega-Mayoral, D. Vella, T. Borzda, M. Prijatelj, I. Tempra, E. A. Pogna, S. Dal Conte, P. Topolovsek, N. Vujicic, G. Cerullo, D. Mihailovic, and C. Gadermaier, "Exciton and charge carrier dynamics in few-layer WS_2," Nanoscale **8**, 5428 (2016).
25. Z. E. Eroglu, O. Comegys, L. S. Quintanar, N. Azam, S. Elafandi, M. Mahjouri-Samani, and A. Boulesbaa, "Ultrafast dynamics of exciton formation and decay in two-dimensional tungsten disulfide (2D-WS_2) monolayers," Phys. Chem. Chem. Phys. **22**, 17385 (2020).
26. A. Brasington, D. Golla, A. Dave, B. Chen, S. Tongay, J. Schaibley, B. J. LeRoy, and A. Sandhu, "Role of defects and phonons in bandgap dynamics of monolayer WS_2 at high carrier densities," J. Phys. Mater. **4**, 015005 (2021).
27. P. D. Cunningham, K. M. McCreary, A. T. Hanbicki, M. Currie, B. T. Jonker, and L. M. Hayden, "Charge trapping and exciton dynamics in large-area CVD grown MoS_2," J. Phys. Chem. C **120**, 5819 (2016).
28. Y. Zhao, Q. Huang, H. Cai, X. Lin, H. He, H. Cheng, T. Ma, and Y. Lu, "Ultrafast control of slow light in THz electromagnetically induced transparency metasurfaces," Chin. Opt. Lett. **19**, 073602 (2021).
29. L. Zhang, J. Liu, W. Gong, H. Jiang, and S. Liu, "Diffraction based single pulse measurement of air ionization dynamics induced by femtosecond laser," Opt. Express **29**, 18601 (2021).
30. Q. Yue, Z. Cheng, L. Han, Y. Yang, and C. Guo, "One-shot time-resolved holographic polarization microscopy for imaging laser-induced ultrafast phenomena," Opt. Express **25**, 14182 (2017).
31. Z. Zhong, L. Zhang, H. Jiang, W. Gong, H. Gu, X. Chen, and S. Liu, "A Brewster incidence method for shocked dynamic metrology of transparent materials and its error evaluation," AIP Adv. **10**, 105203 (2020).

32. H. Tsai, Y. Huang, P. Tsai, Y. Chen, H. Ahn, S. Lin, and Y. Lu, "Ultrafast exciton dynamics in scalable monolayer MoS_2 synthesized by metal sulfurization," ACS Omega **5**, 10725 (2020).
33. Z. Zhong, W. Gong, H. Jiang, H. Gu, X. Chen, and S. Liu, "Investigation of spatial chirp induced by misalignments in a parallel grating pair pulse stretcher," Appl. Sci. **10**, 103110 (2020).
34. M. Palummo, M. Bernardi, and J. C. Grossman, "Exciton radiative lifetimes in two-dimensional transition metal dichalcogenides," Nano Lett. **15**, 2794 (2015).
35. H. Wang, C. Zhang, W. Chan, C. Manolatou, S. Tiwari, and F. Rana, "Radiative lifetimes of excitons and trions in monolayers of the metal dichalcogenide MoS_2," Phys. Rev. B **93**, 045407 (2016).